

ARTICLE



Arsenic trioxide elicits prophylactic and therapeutic immune responses against solid tumors by inducing necroptosis and ferroptosis

Jinfeng Chen^{1,2}, Ziqi Jin^{1,2}, Shuqing Zhang^{1,2}, Xiao Zhang^{1,2}, Peipei Li^{1,2}, Heng Yang^{1,2,3} and Yuting Ma^{1,2,3,4}✉

© The Author(s), under exclusive licence to CSI and USTC 2022

Boosting tumor immunosurveillance with vaccines has been proven to be a feasible and cost-effective strategy to fight cancer. Although major breakthroughs have been achieved in preventative tumor vaccines targeting oncogenic viruses, limited advances have been made in curative vaccines for virus-irrelevant malignancies. Accumulating evidence suggests that preconditioning tumor cells with certain cytotoxic drugs can generate whole-cell tumor vaccines with strong prophylactic activities. However, the immunogenicity of these vaccines is not sufficient to restrain the outgrowth of existing tumors. In this study, we identified arsenic trioxide (ATO) as a wide-spectrum cytotoxic and highly immunogenic drug through multiparameter screening. ATO preconditioning could generate whole-cell tumor vaccines with potent antineoplastic effects in both prophylactic and therapeutic settings. The tumor-preventive or tumor-suppressive benefits of these vaccines relied on CD8⁺ T cells and type I and II interferon signaling and could be linked to the release of immunostimulatory danger molecules. Unexpectedly, following ATO-induced oxidative stress, multiple cell death pathways were activated, including autophagy, apoptosis, necroptosis, and ferroptosis. CRISPR–Cas9-mediated knockout of cell death executors revealed that the absence of *Rip3*, *Mkl1*, or *Acs14* largely abolished the efficacy of ATO-based prophylactic and therapeutic cancer vaccines. This therapeutic failure could be rescued by coadministration of danger molecule analogs. In addition, PD-1 blockade synergistically improved the therapeutic efficacy of ATO-based cancer vaccines by augmenting local IFN- γ production.

Keywords: Tumor vaccine; Arsenic trioxide; Necroptosis; Ferroptosis; Immunosurveillance

Cellular & Molecular Immunology (2023) 20:51–64; <https://doi.org/10.1038/s41423-022-00956-0>

INTRODUCTION

Although the therapeutic approaches for advanced malignancies are being unprecedentedly expanded, there is no doubt that prevention and early intervention are still promising and cost-effective strategies to reduce cancer-related mortality [1]. There is a consensus that maintaining a healthy lifestyle, keeping physically active, and avoiding risky behaviors and exposure to carcinogenic factors are epidemiologic approaches for cancer prevention. It is noteworthy that prophylactic and therapeutic vaccines are also feasible options to reduce cancer incidence and delay tumor progression [2]. For example, prophylactic vaccines targeting oncogenic viruses, such as human papillomavirus or hepatitis B virus, have markedly reduced the risk of cervical cancer and liver cancer, respectively [3, 4]. For virus-irrelevant neoplasms that are much less predictable, therapeutic vaccines have been developed to target tumor-associated antigens or tumor-specific antigens (personalized or shared neoantigens) by delivering nucleic acids (DNA or mRNA), synthetic peptides, recombinant proteins, tumor lysates, or dendritic cells (DCs) pulsed with tumor

antigens [5–9]. These vaccines exhibit clinical safety, but their therapeutic benefits are often limited, mainly due to the low immunogenicity of tumor antigens (compared to highly immunogenic viral antigens) and the immunosuppressive tumor micro-environment (TME) [9, 10].

Unexpectedly, some chemotherapy regimens produce a vaccine-like effect, which not only produces tumoricidal activities but also elicits long-term cancer immunosurveillance [11, 12]. By triggering immunogenic cell death (ICD), certain chemotherapeutic drugs (such as mitoxantrone, oxaliplatin, and doxorubicin) can induce the exposure of tumor antigens and danger molecules (also called ICD factors, such as ATP, HMBG1, CALR, IFN α/β , and ANXA1), thus augmenting the antigenicity and adjuvanticity of tumor cells [13]. Preconditioning with some chemotherapeutic drugs, rather than freeze–thaw cycles, endows dying tumor cells with high immunogenicity [14, 15]. Indeed, subcutaneous delivery of immunogenic drug-treated tumor cells can effectively protect naive immunocompetent mice from subsequent tumor rechallenge [14, 16]. A challenging yet widely applicable scenario would

¹Institute of Systems Medicine, Chinese Academy of Medical Sciences & Peking Union Medical College, Beijing 10005, China. ²Suzhou Institute of Systems Medicine, Suzhou, Jiangsu 215123, China. ³National Key Laboratory of Medical Immunology, Shanghai 200433, China. ⁴Collaborative Innovation Center for Cancer Personalized Medicine, Nanjing Medical University, Nanjing 211166, China. ✉email: yuting_ma1984@163.com

Received: 30 May 2022 Accepted: 7 November 2022

Published online: 30 November 2022

be to therapeutically harness ICD-based whole-cell vaccines against solid tumors. In principle, this vaccination approach offers unique advantages over other therapeutic options. Compared with the direct administration of corresponding drugs, this would be less toxic to nonmalignant cells in tumor-bearing individuals. Compared with vaccines targeting specific epitopes, these vaccines would convey broad coverage of characterized and uncharacterized tumor antigens [17]. This type of naturally multivalent vaccine can be applied regardless of major histocompatibility complex (MHC) identity [18]. Additionally, it can simultaneously trigger CD8⁺ and CD4⁺ T-cell responses and boost tumor eradication [17, 19, 20]. Progress on vaccines incorporating an oncolytic virus or lethally irradiated tumor cells has proven the concept that ICD-based vaccines can be therapeutically efficacious. The therapeutic benefits of these vaccines can be further improved by genetically engineered secretion of immunostimulatory cytokines (such as granulocyte macrophage-colony stimulating factor and vascular endothelial growth factor C) [21, 22]. Although encouraging, biosafety concerns regarding viral pathogenicity, selective tropism for cancerous cells, and the low immunogenicity of tumor cells are intrinsic limitations making it challenging to achieve further breakthroughs [21, 23, 24].

Despite being conceptually appealing, chemotherapeutic drug-preconditioned whole-cell vaccines have not achieved striking therapeutic outcomes in laboratory or clinical investigations [25, 26], suggesting an urgent need for strategic optimization. From a selected panel of antineoplastic drugs, we identified arsenic trioxide (ATO) as a broad-spectrum cytotoxic and highly immunogenic agent. ATO is widely used in first-line therapies for newly diagnosed and relapsed acute promyelocytic leukemia (APL), either alone or in combination with all-trans retinoic acid (ATRA), which revolutionarily makes this lethal malignant disease curable [27, 28]. In our study, we discovered that ATO-treated tumor cells not only showed strong prophylactic activities but also effectively restricted the outgrowth of established tumors. The re-establishment of antitumor immunosurveillance relied on the generation and release of ICD factors upon cellular stress responses and the execution of death programs. Distinct pathways of programmed cell death have long been considered parallel, nonoverlapping events. Surprisingly, we discovered that ATO could sequentially or simultaneously activate multiple key executors involved in different cellular stress and death modalities, indicating possible crosstalk among these events. All these events seemed to be downstream of the ATO-induced accumulation of reactive oxygen species (ROS) and oxidative stress in tumor cells. Previous studies have separately investigated the immunological consequences of autophagy, apoptosis, necroptosis, pyroptosis and ferroptosis in tumor cells [14, 29–33], demonstrating their impacts on antitumor immunity. Similar findings have been confirmed through the “synthetic” elicitation of cellular stress and demise with doxycycline inducible Tet-on systems, as exemplified by triggering necroptosis or endoplasmic reticulum (ER) stress via enforced expression of receptor interacting protein kinase 3 (RIPK3) and reticulon-1C, respectively [34, 35]. In this study, we generated a series of knockout (KO) tumor cell clones with CRISPR-Cas9 technology and addressed the impacts of key cell death executors on the viability, clonogenicity, and immunogenicity of ATO-treated tumor cells. In particular, we explored whether and how these regulators of cell death affected the efficacy of prophylactic and therapeutic whole-cell tumor vaccines. In addition, we discovered that combination of an immune checkpoint inhibitor against PD-1 and an ATO-based therapeutic vaccine generated synergistic benefits against solid tumors.

MATERIALS AND METHODS

Mice and cell lines

Female C57BL/6 (H2K^b), BALB/c (H2K^d) and athymic nude mice aged between 6–8 weeks were ordered from Charles River (Beijing, China).

B6.129S2-Irfar1tm1Agt/Mmjax (*Irfar*^{-/-}, H2K^b) mice were purchased from The Jackson Laboratory and bred in our animal facility as homozygotes. CD45.1⁺ OT-1 mice were obtained from Dr. Xiao Su under MTA authorizations (Institut Pasteur of Shanghai, Chinese Academy of Sciences). All mice were maintained in specific pathogen-free (SPF) conditions under 12-h/12-h light/dark cycles with ad libitum access to food and water. All experimental protocols were approved by the Ethics Committee of the Chinese Academy of Medical Sciences and International Animal Care and Use Committee of the Suzhou Institute of Systems Medicine (No. ISM-IACUC-0075-R). The murine fibrosarcoma cell line MCA805 was established in our laboratory by flow cytometry-based single-cell cloning from 3-methylcholanthrene-induced fibrosarcoma tissues. CT26 colon cancer (H2K^d, CRL-2638), B16-F10 melanoma (H2K^b, CRL-6475), L1210 lymphocytic leukemia (H2K^d, CCL-219), ABE-8.1/2 pre-B lymphoma (H2K^d, TIB-205), EL4 lymphoma (H2K^d, TIB-39), and simian virus 40/T antigen-transformed immortalized mouse embryonic fibroblasts (WT SV40 MEFs, CRL-2907) were purchased from ATCC (Beijing Zhongyuan Ltd.). TC-1 lung cancer (H2K^b) and MCA205 fibrosarcoma (H2K^b) cells were kindly provided by Dr. Guido Kroemer (Centre de Recherche Des Cordeliers, INSERM U1138, France). Eμ-Myc p19 *Arf*^{-/-} mouse lymphoma cells were generously provided by Dr. Hai Jiang (State Key Laboratory of Cell Biology, Chinese Academy of Sciences). All cell lines were cultured in high-glucose DMEM supplemented with L-glutamine, HEPES (01–172–1A, Biological Industries) 10% FBS (FBS-12A, CAPRICORN) and 100 U mL⁻¹ penicillin/streptomycin (5140163, Gibco) at 37 °C with 5% CO₂. Adherent cells were passaged with 0.25% trypsin-EDTA (BL512A, Biosharp) when they reached 80–90% confluency. All cell lines and primary cell cultures were routinely tested to avoid contamination with mycoplasma.

Cell death, cell cycle and clonogenicity assays

For drug screening, MTX (M6545, Sigma), DNR (HY-13062, MCE), VNR (HY-12053A, MCE), EPI (HY-13624A, MCE), OXA (HY-17371, MCE), DOX (D1515, Sigma), CDDP (S1166, Selleck), VCR (HY-N0488A, MCE), ART (HY-B0094, MCE), and COL (HY-16569, MCE) were used at the indicated time points and doses. Tumor cells were seeded at 10⁴ cells per well in 96-well plates. CCK-8 solution (MG6432, MESGEN) was added at 10 μL per 100 μL culture medium for each well. After a 2-hour incubation at 37 °C, the conversion of WST-8 to formazan by viable cells was measured by assessing the optical density (O.D.) at 450 nm and 570 nm with the SpectraMax[®] i3 Platform from Molecular Devices[®]. Alternatively, the intracellular ATP content was used to detect metabolically active cells using the CellTiter-Glo[®] Luminescent Cell Viability Assay (G9242, Promega). Cell death was also quantified by dual staining with Annexin V (indicating phosphatidylserine exposure, 640947, BioLegend) and DAPI (2 μg mL⁻¹, A606584, Sangon Biotech) or double staining with DAPI and YO-PRO-1 (indicating early-stage cell membrane permeability, 5 μM, Y3606, Thermo Fisher Scientific). To evaluate the cell cycle, ATO-treated cells (25 μM, 8 h) were fixed in 70% ethanol at 4 °C overnight, washed twice in 1xPBS, and subsequently labeled with a propidium iodide/RNase staining buffer (550825, BD Pharmingen). Flow cytometry was used to analyze these data (Attune NxT Flow Cytometer, Life Technologies). For colony formation assays, tumor cells were seeded in 12-well plates at the indicated confluency and treated with ATO at the indicated time points and doses. The cells were then trypsinized and suspended in fresh medium. One hundred live tumor cells (negative for trypan blue staining) were seeded in 6-well plates and cultured for 8 days. The resultant colonies were stained with 0.5% crystal violet solution (G1062, Solarbio), imaged, and quantified by ImageJ software (NIH, Bethesda, MD, USA).

Murine tumor models

TC-1 cells were treated with 25 μM ATO or 2 μM MTX for 16 h, washed twice with 1x PBS, and inoculated subcutaneously (10⁶ cells per mouse) into naïve mice (as prophylactic vaccines) or tumor-bearing mice (as therapeutic vaccines). Alternatively, TC-1 cells were exposed to 50 Gy X-ray irradiation (in a total of 6 min) or three rounds of freeze–thaw cycles. MCA805 cells or muscle cells freshly isolated from the thigh were treated with 25 μM ATO. These dying cells were used as experimental controls. Their protective effects against subsequent tumor cell rechallenge (for prophylactic vaccines) or the outgrowth of established tumors (for therapeutic vaccines) were monitored 2–3 times per week. In some experiments, antibodies targeting immune cell subsets, cytokines or their receptors, or immune checkpoint molecules were administered at the indicated time points; these included antibodies targeting CD8 (53–6.7), NK1.1 (PK136), IFNAR-1 (MAR1-5A3), IFN-γ (XMG1.2), and PD-1 (RMP1-14).

All antibodies were purchased from BioXCell. For ATO-based chemotherapy, an ATO solution (0.01 mg kg⁻¹, 0.125 mg kg⁻¹, or 0.25 mg kg⁻¹ body weight in 40 µL PBS) was injected intratumorally at the indicated time points. In some settings, an ATO-based *Rip3*^{-/-} whole-cell vaccine was mixed with the apyrase inhibitor ARL67156 (3.2 mg kg⁻¹, A265, Sigma), TLR4 agonist MPLAs (0.5 mg kg⁻¹, tlr1-mpls, InvivoGen), or STING agonist 2'3'-cGAMP (0.5 mg kg⁻¹, tlr1-nacga23-01, InvivoGen) before subcutaneous injection.

Detection of ICD factors, ROS generation, and lipid peroxidation

To quantify the release of ATP and HMGB1, 5 × 10⁴ cells/well were seeded in a 48-well plate in 300 µL DMEM, and cell supernatants were collected and centrifuged at 500 × g for 5 min to remove cell debris at the indicated time points. Extracellular ATP was detected by a bioluminescent assay kit (FLAA, Sigma Aldrich). The HMGB1 level was measured by an ELISA kit (ST51011, IBL International). To quantify extracellular cGAMP, tumor cells (90% confluent) seeded in 6-well plates were treated with 25 µM ATO for 8 h. The supernatant was lyophilized, dissolved in 100 µL ddH₂O, and quantified with an ELISA kit (501700, Cayman). To detect type I IFN production by dying tumor cells, ATO-treated tumor cells were washed with 1 × PBS and cocultured with the fibroblast cell line L929-ISRE (expressing an interferon-stimulated responsive element) for 4 h. The cells were then lysed and analyzed with a Dual-luciferase Reporter Assay System (E1960, Promega) using a SpectraMax[®] L Luminometer. Surface CALR was stained with a rabbit monoclonal antibody (1:500, clone EPR3924, Abcam), followed by staining with Alexa 647-conjugated goat anti-rabbit IgG (H + L) (1:500, A-21245, Life Technologies). Tumor cells were treated with 25 µM ATO, with or without 5 mM NAC (HY-130215, MCE), followed by incubation with 1 µM DCFH-DA (ab113851, Abcam) or 1 µM BODIPY 581/591 C11 (D3861, Thermo Fisher Scientific) at 37 °C for 30 min. The fluorescent signals from DCF and BODIPY were analyzed by flow cytometry (Attune NxT Flow Cytometer, Life Technologies).

Seahorse real-time cell metabolism

Cells were seeded at 5 × 10⁴ cells per well in 24-well XF cell culture microplates. After 8 h of treatment with ATO (25 µM), the extracellular acidification rate (ECAR) was tested by the sequential addition of 10 mM glucose, 0.5 µM oligomycin, and 100 mM 2-deoxyglucose (2-DG). The oxygen consumption rate (OCR) was measured by the sequential injection of 1 µM oligomycin, 1.5 µM fluoro-carbonyl cyanide phenylhydrazine (FCCP), and 100 nM rotenone plus 1 µM antimycin A according to the manufacturer's instructions (Seahorse XFe24, Agilent Technologies).

Statistical analyses

The required sample sizes were estimated according to our previous experience with similar experiments. Age- and sex-matched mice were randomly assigned to different groups. Statistical analyses and graph generation were performed with GraphPad Prism 8 (San Diego, CA, USA). All results are presented as the means ± SEMs, of at least five parallel assessments. All experiments were repeated independently at least twice. Tumor progression curves were compared by calculating the area under the curve (AUC) for individual mice. Statistical differences were determined using an unpaired two-tailed Student's *t* test or the Mann–Whitney *U* test. Log-rank tests were applied to analyze Kaplan–Meier survival curves. The strength of the association between two variables and the direction of the relationship were evaluated with nonparametric correlation coefficient analyses (Spearman), and the one-tailed *P* value was calculated.

RESULTS

Drug screening reveals ATO as a highly immunogenic and broad-spectrum cytotoxic agent for tumor cells

Previous studies suggest that the immunogenic properties of antineoplastic drugs can be quite different. With biomarker detection in vitro and functional validation in vivo, some drugs have been identified as ICD inducers that can both kill tumor cells and stimulate antitumor immunity [36]. With a cell viability assay based on dehydrogenase activities, we compared the cytotoxicities of daunorubicin (DNR), vinorelbine (VNR), epirubicin (EPI), vincristine (VCR), cisplatin (CDDP), ATO, artemisinin (ART), colchicine (COL), doxorubicin (DOX), mitoxantrone (MTX), and

oxaliplatin (OXA) to TC-1 lung cancer cells. All drugs could efficiently kill TC-1 cells in a dose- and time-dependent manner, except CDDP, VCR, COL, and ART (Fig. 1A). Quantification of the intracellular ATP content suggested that DNR and ATO led to the largest reductions in cell viability (Fig. 1B). To screen for potent ICD inducers, ovalbumin (OVA)-expressing TC-1 cells were pretreated with the highly cytotoxic drugs identified in these viability assays and injected subcutaneously into the footpad of naïve C57Bl/6 mice. Their capability to prime OVA-specific OT-1 T cells in the popliteal lymph nodes (LNs) was analyzed by flow cytometry. Compared with repeated freeze–thaw cycles (F/T), preconditioning with drugs (particularly ATO, DOX, and OXA) made tumor cells more immunogenic, as illustrated by the observed accelerated OT-1 cell proliferation (Fig. 1C, S1A, B). In another functional assay, dying tumor cells were cocultured with bone marrow-derived DCs (BMDCs) to mimic tumor antigen presentation ex vivo, which stimulated IFN-γ production by antigen-specific T cells. Consistently, TC-1 OVA cells pretreated with ATO or DOX led to the highest secretion of IFN-γ by OT-1 cells (Fig. 1D). In summary, these results revealed ATO as a strong ICD inducer. Additionally, ATO showed wide-spectrum toxicity to both solid and hematopoietic tumor cells, as indicated by disrupted membrane integrity, phosphatidylserine (PS) exposure, and cell cycle arrest (Fig. 1E, S1C). As expected, the ATO-induced decreases in cell viability and clonogenicity were dependent on the dose and duration of drug treatment (Fig. 1F, G). However, increased confluency of tumor cells seemed to facilitate their resistance to ATO (Fig. 1H). Finally, colony-forming assays demonstrated that 16 h of treatment with ATO at 25 µM completely abolished the clonogenicity of tumor cells, even if the cells were seeded at a high density (Fig. 1I, S1D). A CCK-8 assay also confirmed that ATO-preconditioned tumor cells completely lost their proliferative capabilities (Fig. S1E).

ATO-based whole-cell vaccine elicits antitumor immunity and exhibits prophylactic activities against solid tumors

We continued to test whether subcutaneous injection of ATO-treated dying tumor cells could trigger tumor-preventive immunity (Fig. 2A). Similar to PBS-treated cells, F/T procedure-treated TC-1 cells failed to protect naïve mice from developing tumors upon rechallenge with live TC-1 cells. However, ATO preconditioning endowed dying TC-1 cells with strong prophylactic activities, which were comparable with those of the MTX-treated whole-cell vaccine (Fig. 2B, S2A). This finding could be reproduced in murine fibrosarcoma models (MCA205 and MCA805) and a colon cancer model (CT26) (Fig. 2C, S2B–D). The prophylactic benefits of the ATO-based vaccine against TC-1 lung cancer required the presence of T cells, particularly CD8⁺ T cells (rather than NK cells), as proven by experiments performed with athymic nude mice and antibody-based cell depletion (Fig. 2D, E, S2E–G). Genetic defects in or antibody-based blockade of type I or type II IFN pathways also abolished the tumor-protective effect of this vaccine regimen (Fig. 2F, G, S2H, I). Importantly, similar findings were consistently observed in the MCA205 and MCA805 fibrosarcoma models, as well as the CT26 colon cancer model (Fig. 2H–L, S2J–N).

ATO potentially triggers the exposure or release of ICD factors

Mechanistic explanations of how dying tumor cells elicit antitumor immunity have been gradually elucidated, among which pattern recognition receptor (PRR)-dependent immune detection of ICD factors from dying tumor cells is of vital importance. Indeed, ATO treatment caused the leakage of intracellular ATP and the nuclear protein HMGB1 into the extracellular milieu (Fig. 3A, B). It triggered the translocation of CALR from the ER lumen to the plasma membrane (Fig. 3C, D), boosted the production of IFN-α/β (Fig. 3E), enhanced the release of the cyclic dinucleotide cGAMP (Fig. 3F), and enhanced the transcription of interferon-stimulated genes (ISGs) (Fig. S3A–D). The expression of ISGs largely relied on the stimulator of interferon genes (STING) pathway, while the STING

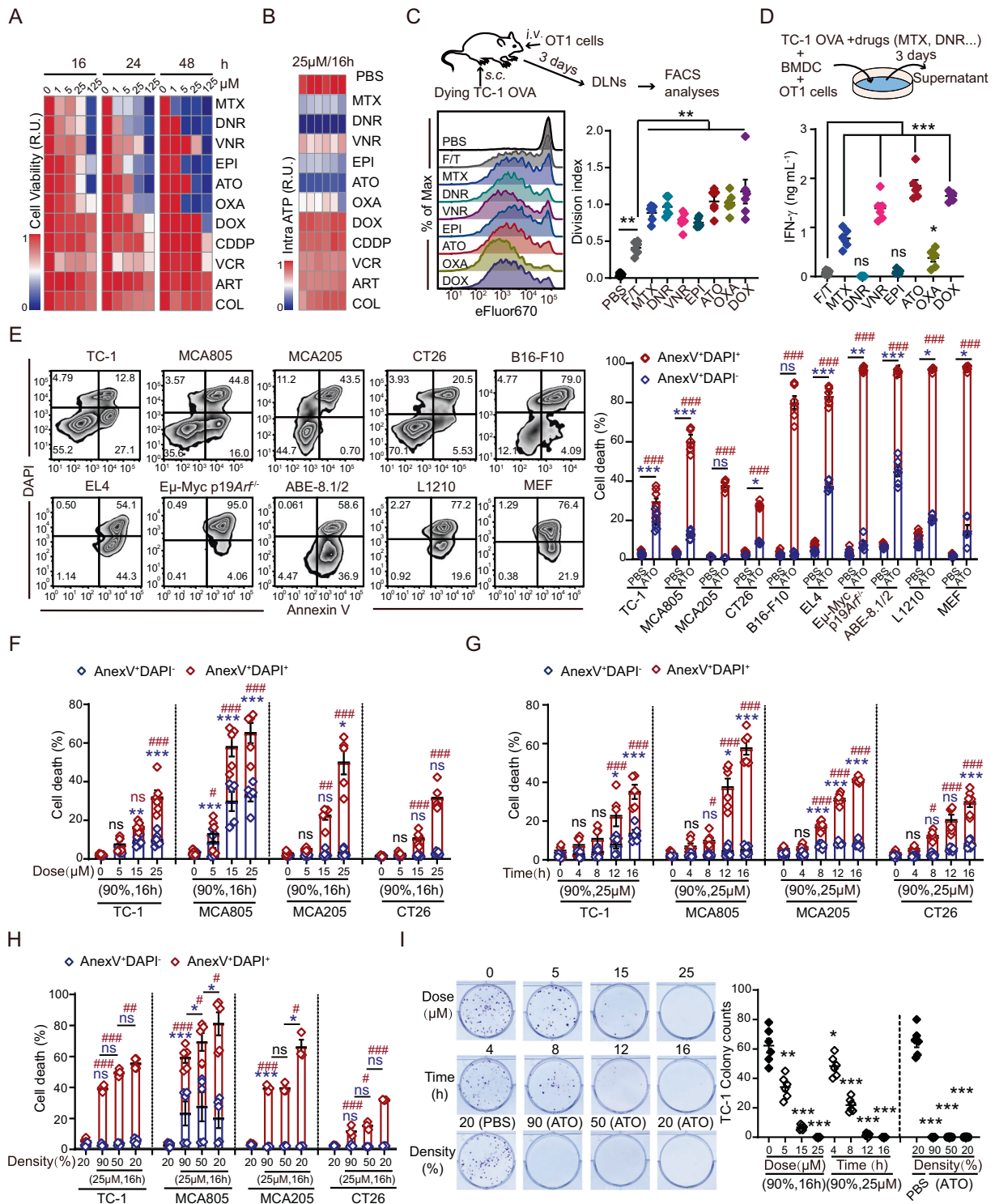


Fig. 1 Multiparameter screening of drugs with high cytotoxicity and immunostimulatory properties. **A** Comparison of drug cytotoxicity to TC-1 cells at the indicated doses and time points measured with CCK-8 assays. R.U. (Relative unit) was calculated from the average O.D. values in each condition as the indicator of cell viability ($n = 3$). **B** The intracellular ATP content was quantified by a CellTiter-Glo[®] luminescent kit after 16 h of treatment with 25 μ M of each drug ($n = 6$). **C** TC-1 OVA cells were treated with the indicated drugs (25 μ M, 16 h) or freeze–thaw cycles (F/T) and injected s.c. into the footpad of mice to stimulate eFluor670-prelabeled OT-1 cells. Typical histograms of OT-1 cell proliferation and statistical analyses of the OT-1 cell division index are shown ($n = 6$). **D** Dying TC-1 cells were cocultured with BMDCs and OT-1 cells. IFN- γ levels in the supernatant were detected by ELISA 3 days later ($n = 6$). **E** The cytotoxicity of ATO (25 μ M, 16 h) to different cell lines was quantified by Annexin V/DAPI staining. Typical cytofluorometric dot plots and statistical analyses are shown ($n = 6$). **F–I** The dose-, time-, and cell density-dependent cytotoxicity of ATO was measured by flow cytometry and colony formation assays with the indicated tumor cell lines ($n = 6$). Data were analyzed by an unpaired, two-tailed Student's t test and are shown as the means \pm SEMs. Data are representative of at least three independent experiments. * or # $p < 0.05$, ** or ## $p < 0.01$, *** or ### $p < 0.001$; ns not significant

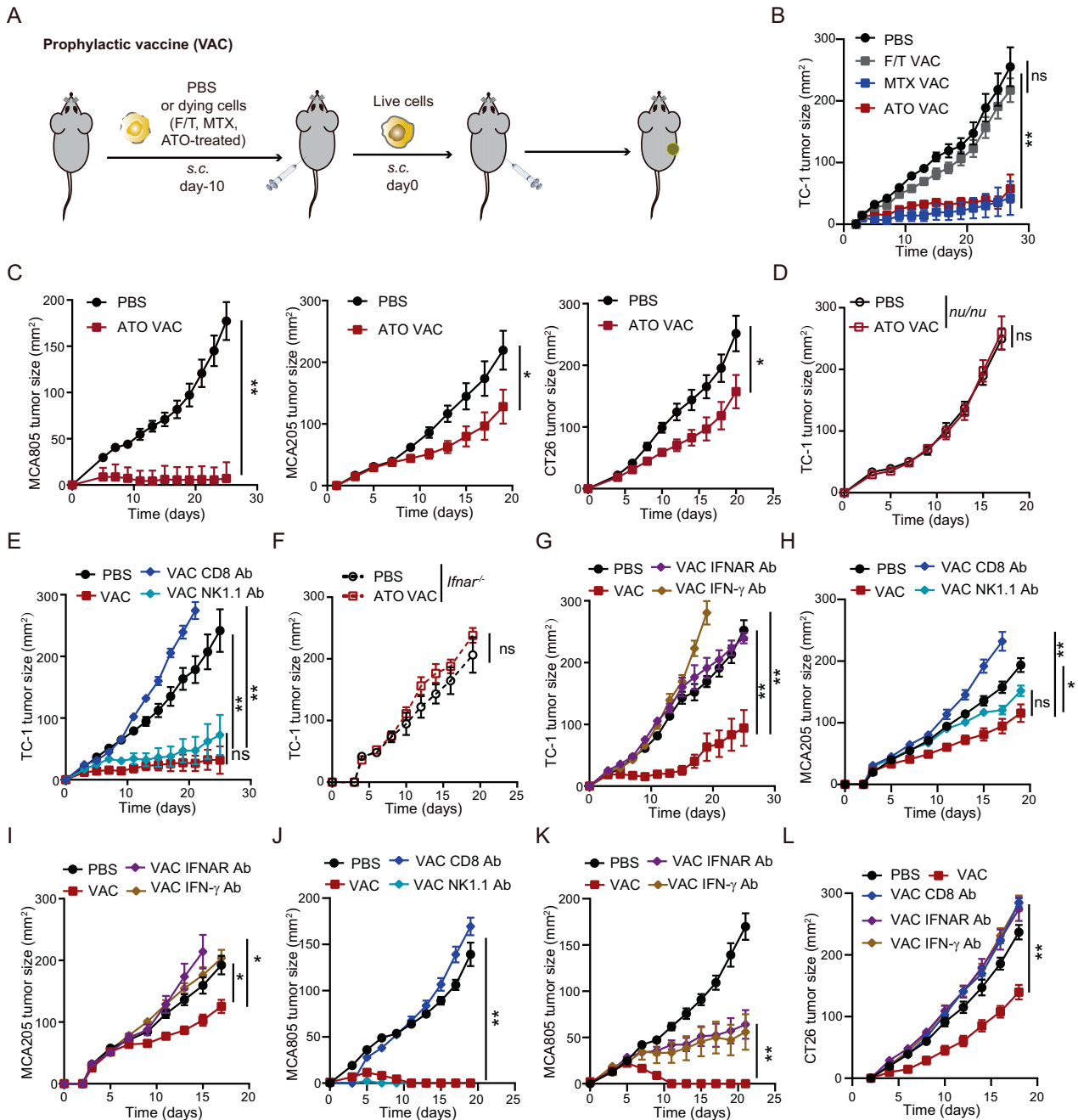


Fig. 2 Prophylactic activities of an ATO-based whole-cell vaccine. **A** Schematic diagram showing the prophylactic tumor vaccine regimen. **B, C** Mice were vaccinated with ATO-pretreated dying tumor cells (TC1, MCA805, MCA205 or CT26 cells) and rechallenged with the corresponding live tumor cells 10 days later. Tumor growth kinetics were monitored for each group ($n = 5-6$). **D-G** The efficacy of an ATO-based whole-cell vaccine against TC-1 lung cancer was compared among athymic *nu/nu* mice (**D**, $n = 6$), WT C57BL/6 mice (**E, G**, $n = 5-7$), and *Ifnar^{-/-}* mice (**F**, $n = 4$). Antibodies were administered to deplete CD8⁺ T cells or NK cells (**E**) or to block type I or II IFN signaling (**G**). **H-L** Kinetics of MCA205 (**H, I**), MCA805 (**J, K**) or CT26 (**L**) tumor growth in mice that had received ATO-based prophylactic vaccines with or without depletion or blocking antibody treatment ($n = 5-8$). All data are shown as the mean \pm SEM. Tumor growth was quantified by calculating the area under the curve (AUC) and analyzed with the unpaired Mann-Whitney *U* test. * $p < 0.05$, ** $p < 0.01$, *** $p < 0.001$; ns not significant

antagonist H151 significantly attenuated the ATO-induced expression of ISGs (Fig. 3G, H). In summary, ATO can be classified as a potent ICD inducer for cancer cells.

ATO induces ROS generation and activates multiple cellular stress and death modalities

With transcriptomic profiling of TC-1 and MCA805 cells by RNA sequencing, we noticed that genes that were commonly

upregulated by ATO in both cell lines could be annotated to several gene ontology (GO) terms, including oxidative phosphorylation, cellular response to stimuli, and response to oxidative stress (Fig. 4A, S4A). Prompted by this finding, we examined the level of oxidative stress in tumor cells with H2DCFDA (a cell-permeant probe for ROS) and BODIPY (a lipid peroxidation sensor). ATO treatment led to a significant shift in the fluorescent intensity of DCF (converted from its nonfluorescent precursor H2DCFDA)

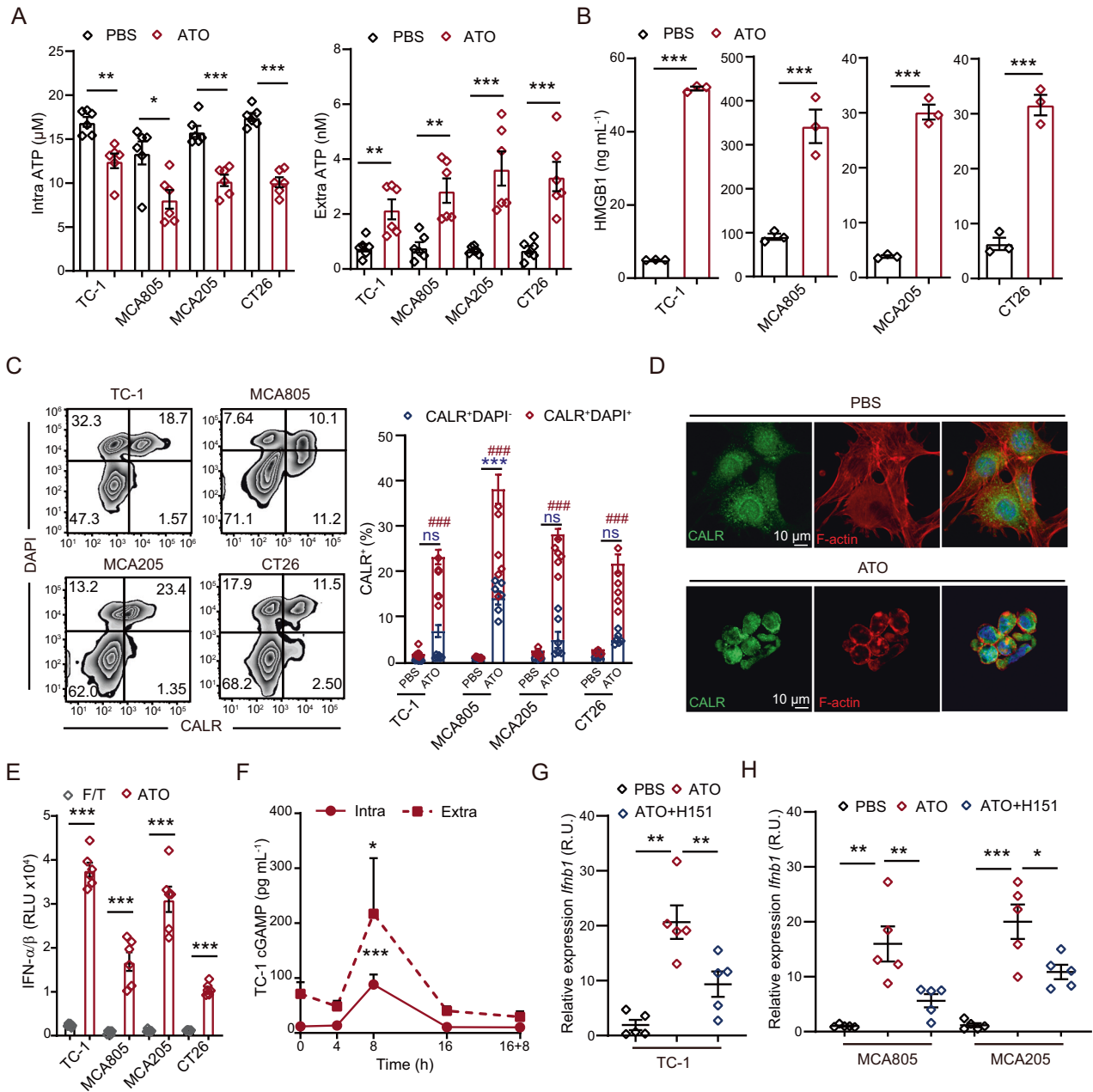


Fig. 3 ATO liberates ICD factors from malignant cells. **A** Intracellular and extracellular ATP concentrations under PBS and ATO (25 μM , 16 h) conditions were compared in TC-1, MCA805, MCA205, and CT26 tumor cells ($n = 6$). **B** HMGB1 release into the extracellular milieu was quantified under PBS and ATO (25 μM , 16 h) conditions for the indicated cell lines ($n = 3$). **C** The ATO-induced surface exposure of CALR was analyzed in DAPI⁺ and DAPI⁻ cell fractions. Representative zebra plots and statistical analyses are shown ($n = 6$). **D** Immunofluorescence staining for CALR and F-actin to evaluate ATO-induced CALR translocation in TC-1 cells. **E** The type I IFN production of tumor cells upon F/T cycles or ATO treatment (25 μM , 16 h) was measured by a L929-ISRE luciferase reporter system ($n = 6$). **F** Kinetics study of the intracellular and extracellular cGAMP content of TC-1 cells following ATO stimulation (25 μM) ($n = 3$). **G**, **H** The level of *Ifnb1* transcription in TC-1 (**G**), MCA805 and MCA205 cells (**H**) upon ATO treatment in the presence or absence of the STING antagonist H151. *Ppia* was used as the house-keeping control for qRT-PCR. Relative expression was calculated as the fold change by means of the $2^{-\text{ddct}}$ method ($n = 6$). All data are shown as the mean \pm SEM. * $p < 0.05$, ** $p < 0.01$, *** or ### $p < 0.001$; ns not significant

and BODIPY (switched from red to green fluorescence), which was blocked by the ROS-scavenging reagent N-acetyl-L-cysteine (NAC) (Fig. 4B, S4B). Since ATO is highly cytotoxic to tumor cells, we were curious about the principal pathways that contribute to cell death. The basal-level expression of multiple cell death executors was examined by western blotting (WB), including (1) Beclin 1 (BECN1), autophagy-related protein 5 (ATG5), and ATG7, which are essential for autophagy; (2) Caspase 3 (CASP3) and CASP8, which are involved in apoptosis and pyroptosis; (3) Gasdermin E (GSDME)

and GSDMD, which mediate pyroptosis; (4) ACSL4 and GPX4, which regulate ferroptosis; and (5) RIP3 and MLKL, which modulate necroptosis. All these cell death executors could be detected in TC-1 and MCA805 cells. However, RIP3 was barely detectable in CT26 and MCA205 cells (Fig. 4C).

Since TC-1 cells were 'fully equipped' with all these cell death machineries, we further investigated which cell death pathways can be activated by ATO. Kinetic studies showed that characteristic markers of autophagy, light chain 3 (LC3) lipidation and

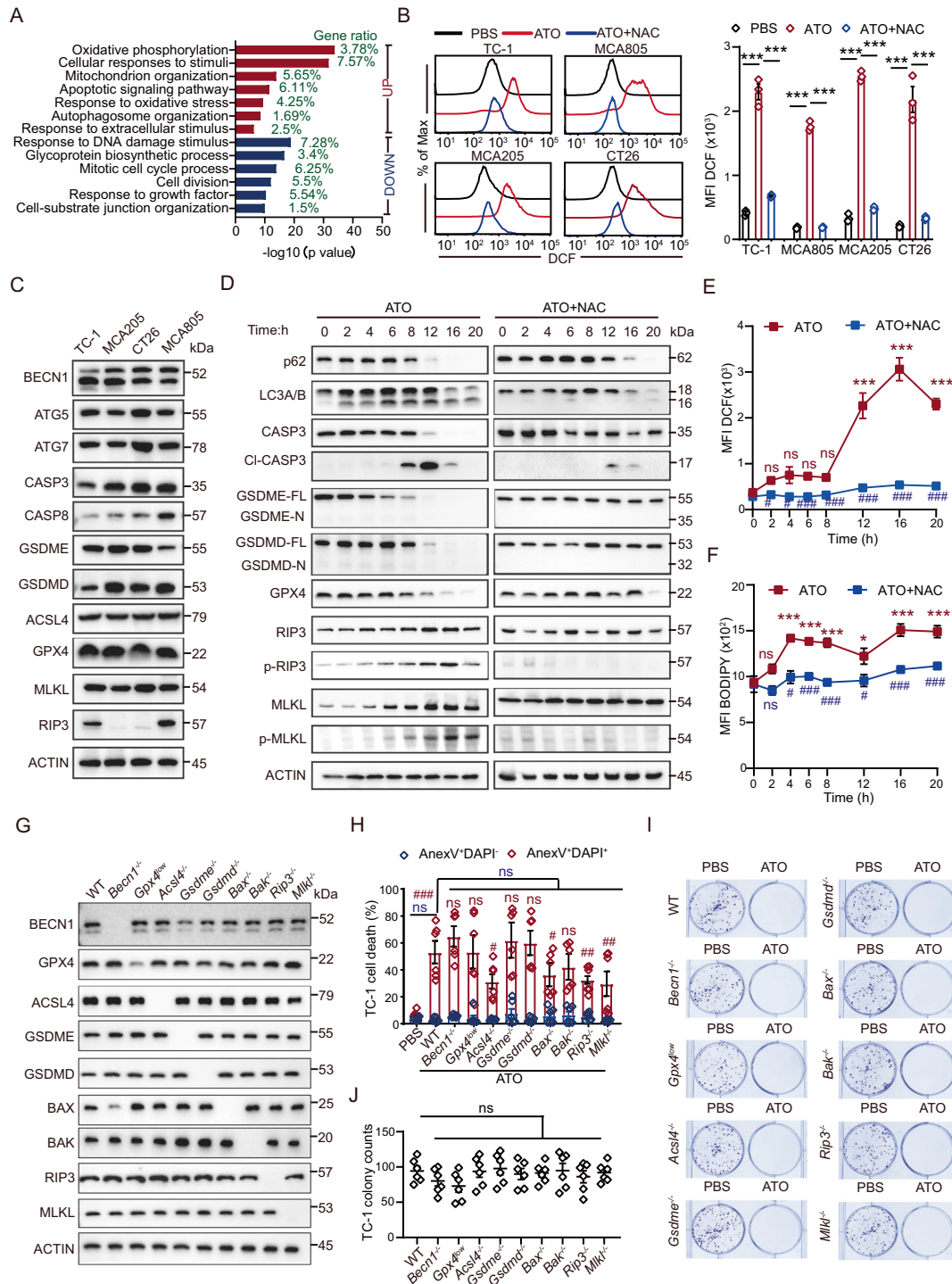


Fig. 4 ATO triggers oxidative stress and activates multiple cell death executors. **A** Gene ontology analyses of commonly up- or downregulated genes in TC-1 and MCA805 cells upon ATO (25 μ M, 16 h) treatment. **B** Flow cytometry-based evaluation of ATO-induced ROS generation and its blockade by NAC preconditioning. Representative histograms and statistical analyses of the mean fluorescence intensity (MFI) are shown ($n = 3$). **C** The expression of autophagy executors (BECN1, ATG5, and ATG7), apoptosis or pyroptosis executors (CASP3, CASP8, GSDME, and GSDMD), ferroptosis executors (ACSL4 and GPX4), and necroptosis executors (RIP3 and MLKL) was measured by semiquantitative WB. **D** Kinetics study of the ATO-triggered activation of major cell death executors in TC-1 cells, including p62 degradation, LC3 lipidation, CASP3 cleavage (CI-CASP3), N-terminal fragment generation from full-length GSDME and GSDMD, GPX4 degradation, and RIP3 and MLKL phosphorylation (left panel). Similar readouts were detected in the presence of the ROS scavenger NAC (right panel). **E, F** Kinetics analyses of the ATO-induced ROS generation (**E**) and lipid peroxidation (**F**) in TC-1 cells with or without NAC treatment. Statistics are shown for ATO versus PBS (marked with *) and ATO + NAC versus ATO (marked with #) ($n = 3$). **G** Genes encoding key cell death executors were individually deleted with CRISPR-Cas9 technologies and validated by WB. **H–J** ATO-induced cell death in WT cells and all KO clones was measured by evaluating the frequency of Annexin V⁺DAPI⁻ and Annexin V⁺DAPI⁺ cells (**H**, $n = 6$) or performing colony formation assays (**I, J**, $n = 6$). All data are shown as the mean \pm SEM. * or # $p < 0.05$, ** or ## $p < 0.01$, *** or ### $p < 0.001$; ns not significant

sequestosome 1 (p62/SQSTM1) degradation, could be observed over time, starting at 2 h, and peaked between 8 and 12 h. Cleavage of CASP3 appeared at 8 h and peaked at 12 h, indicating the onset of apoptosis and/or pyroptosis [37, 38]. As a classic caspase-3 substrate during apoptosis, PARP was cleaved between 4–20 h (Fig. S4C). Although full-length (FL) GSDME and GSDMD were gradually degraded after ATO treatment, the cytotoxic N-terminal domains of GSDME and GSDMD were undetectable at all time points (Fig. 4D). In contrast, tumor necrosis factor α (TNF- α) plus cycloheximide (CHX) effectively induce the cleavage of the N-terminal domain from full-length GSDME (Fig. S4C). ASC speck formation can be used as a biomarker for inflammasome activation [39]. We found that the number of ASC specks was not increased by ATO treatment, as revealed by immunofluorescence staining (Fig. S4D). Therefore, ATO failed to trigger pyroptosis, while activation of CASP3 might represent only an ongoing apoptotic process. In the presence of the pancaspase inhibitor Z-VAD, the autophagosome-lysosome fusion inhibitor bafilomycin A1, or the proteasome inhibitor MG132, the ATO-induced degradation of full-length GSDME was not blocked. The N-terminal fragments of GSDME remained undetectable in the presence of these inhibitors (Fig. S4C). ATO rapidly induced the phosphorylation of RIP3 and MLKL, starting between 4 and 6 h and peaking at 16 h, indicating that necroptosis may also contribute to the cytotoxic activity of ATO. Moreover, ATO resulted in the degradation of glutathione peroxidase 4 (GPX4), a major scavenger of phospholipid hydroperoxides, starting from 6–8 h (Fig. 4D). Noticeably, ATO-triggered oxidative stress seemed to be a prerequisite for switching on these cell death executors, since the NAC-based clearance of ROS dramatically blocked their activation and lipid peroxidation and inhibited cell death (Fig. 4D–F, S4E).

Due to the similar or overlapping activation kinetics of different cell death executors, we speculated on the possibility of crosstalk among corresponding cell death pathways. To dissect the relative contribution of each pathway to cell death, we performed CRISPR–Cas9-based genome editing on parental TC-1 cells and generated a series of KO cell clones lacking each death executor. Specific deletion of target genes was validated by DNA sequencing, quantification of corresponding proteins, and various functional assays (Fig. 4G, S4F–H). Importantly, the absence of *Acsl4*, *Bax*, *Rip3*, or *Mkl1*, but not the other executors, partially reduced the cytotoxicity of ATO (Fig. 4H). However, ROS generation following ATO stimulation was unaffected in all KO cell clones compared with WT parental cells (Fig. S4I), indicating that the absence of downstream cell-death executors did not affect the upstream event of oxidative stress. Additionally, the clonogenicity of TC-1 parental cells and individual KO clones was comparable and was equally abolished by ATO (Fig. 4I, J).

The impacts of different cell death executors on ATO-induced ICD and prophylactic vaccine efficacy

With all the KO cell clones, we were able to address the relative contribution of each cell death executor to ATO-induced ICD. As ATO treatment completely abolished the colony-forming capabilities of both parental TC-1 cells and KO cell clones, ATO-treated tumor cells should not develop tumors in vivo. Therefore, we utilized ATO-treated dying tumor cells as prophylactic whole-cell vaccines and compared their immunogenicity in vivo. The absence of *Becn1*, *Bax*, or *Bak* in tumor cells partially attenuated the tumor-suppressive activities of prophylactic vaccines, while deficiency in *Acsl4* (but not *Gpx4*), *Rip3*, or *Mkl1* completely abrogated the prophylactic effects of whole-cell vaccines (Fig. 5A, S5A). Genetic defects in *Gsdme* or *Gsdmd* did not affect the tumor growth-inhibitory activities of this vaccine regimen (Fig. 5A, S5A–C). To explore the underlying mechanisms governing the uneven contributions of different cell death executors to vaccination outcomes, WT and KO TC-1 cells were engineered to

overexpress the antigen OVA at comparable levels (Fig. S5D) and used to prime OT-1 cells in vivo. In this setting, we observed that the frequency of adoptively transferred OT-1 cells was the lowest in the popliteal LNs of mice receiving *Acsl4*^{-/-}, *Rip3*^{-/-}, or *Mkl1*^{-/-} whole-cell vaccines. Consistently, OT-1 cell proliferation was also largely blocked in these groups (Fig. 5B).

Furthermore, we explored the impact of each cell death executor on ICD factors. The ATO-induced accumulation of extracellular ATP was significantly reduced in the *Becn1*^{-/-}, *Acsl4*^{-/-}, *Gsdme*^{-/-}, *Bax*^{-/-}, *Bak*^{-/-}, *Rip3*^{-/-}, and *Mkl1*^{-/-} groups compared with the corresponding WT groups, indicating the importance of autophagy, apoptosis, necroptosis, and ferroptosis during this process (Fig. 5C, upper panel). Since RIP3 deficiency did not affect the oxidative metabolism (OCR) or glycolysis (ECAR) of tumor cells (Fig. S5E, F), the necroptosis pathway seemed to affect ATP release rather than ATP biogenesis. Most cell death executors seemed to be irrelevant to ATO-induced HMGB1 release, except for *Rip3* and *Mkl1*, suggesting the critical role of the necroptosis pathway in this process (Fig. 5C, lower panel). The absence of *Acsl4*, *Bax*, *Bak*, *Rip3*, or *Mkl1* dramatically inhibited the ATO-triggered exposure of CALR on the plasma membrane, implying indispensable roles for ferroptosis, apoptosis, and necroptosis in generating this ‘eat-me’ signal (Fig. 5D, S5G). Interestingly, we found that *Acsl4*, *Rip3*, and *Mkl1* were necessary for the ATO-induced elevation in the extracellular cGAMP (a STING agonist) level, consistent with the diminished secretion of IFN- β and transcription of ISGs in these KO clones compared with WT TC-1 cells (Fig. 5E, F, S5H). As the expression of ectonucleotide pyrophosphatase/phosphodiesterase 1 (*Enpp1*, a bifunctional enzyme that degrades ATP and cGAMP) was comparable in *Acsl4*^{-/-}, *Rip3*^{-/-}, *Mkl1*^{-/-} and WT cells, with or without ATO treatment, ferroptosis and necroptosis might participate in the generation and/or release of cGAMP rather than cGAMP degradation (Fig. S5I).

The ferroptosis and necroptosis pathways share some common morphological changes, ending in the rupture of the plasma membrane, which can be a limiting step in the release of ICD factors. Indeed, cell membrane integrity upon ATO treatment was better preserved in *Acsl4*^{-/-}, *Rip3*^{-/-}, and *Mkl1*^{-/-} cells than in WT cells, as detected by double-staining with the plasma membrane-permeant dye YO-PRO1 and DAPI (Fig. 5G, S5J). Remarkably, BMDCs loaded with ATO-treated OVA-expressing *Acsl4*^{-/-}, *Rip3*^{-/-}, or *Mkl1*^{-/-} TC-1 cells, but not other KO cells or WT cells, failed to prime IFN- γ production by OT-1 cells (Fig. 5H). All the above results demonstrated that *Rip3*- and *Mkl1*-dependent necroptosis and *Acsl4*-dependent ferroptosis played vital roles in the ATO-induced ICD of cancer cells and the prophylactic activities of these cells.

Executors of necroptosis and ferroptosis are required for the therapeutic activities of ATO-based whole-cell vaccines

We further explored the therapeutic potential of a chemotherapeutic drug-preconditioned whole-cell vaccine against established tumors (Fig. 6A). Although ATO has been clinically approved with the goal of curing APL, its therapeutic benefits against solid tumors are still limited [40, 41]. Indeed, intratumoral injection of ATO failed to suppress the outgrowth of TC-1 and MCA205 tumors in vivo (Fig. 6B, S6A–C), even when applied at high doses (Fig. S6D, E). Although MTX-treated tumor cells exhibited strong prophylactic activities, they were not sufficient to reduce the progression of established tumors. In contrast, one immunization with an ATO-based whole-cell vaccine caused a substantial decline in the growth kinetics of both TC-1 tumors and MCA805 tumors (Fig. 6C, D, S6F, G). This therapeutic outcome largely relied on type I IFN signaling in mice (Fig. 6E, S6H). Importantly, subcutaneous injection of ATO-treated nonmalignant muscle cells or MCA805 cells or irradiated TC-1 tumor cells did not delay the progression of existing TC-1 tumors. Only ATO-treated TC-1 cells exhibited tumor growth-inhibitory

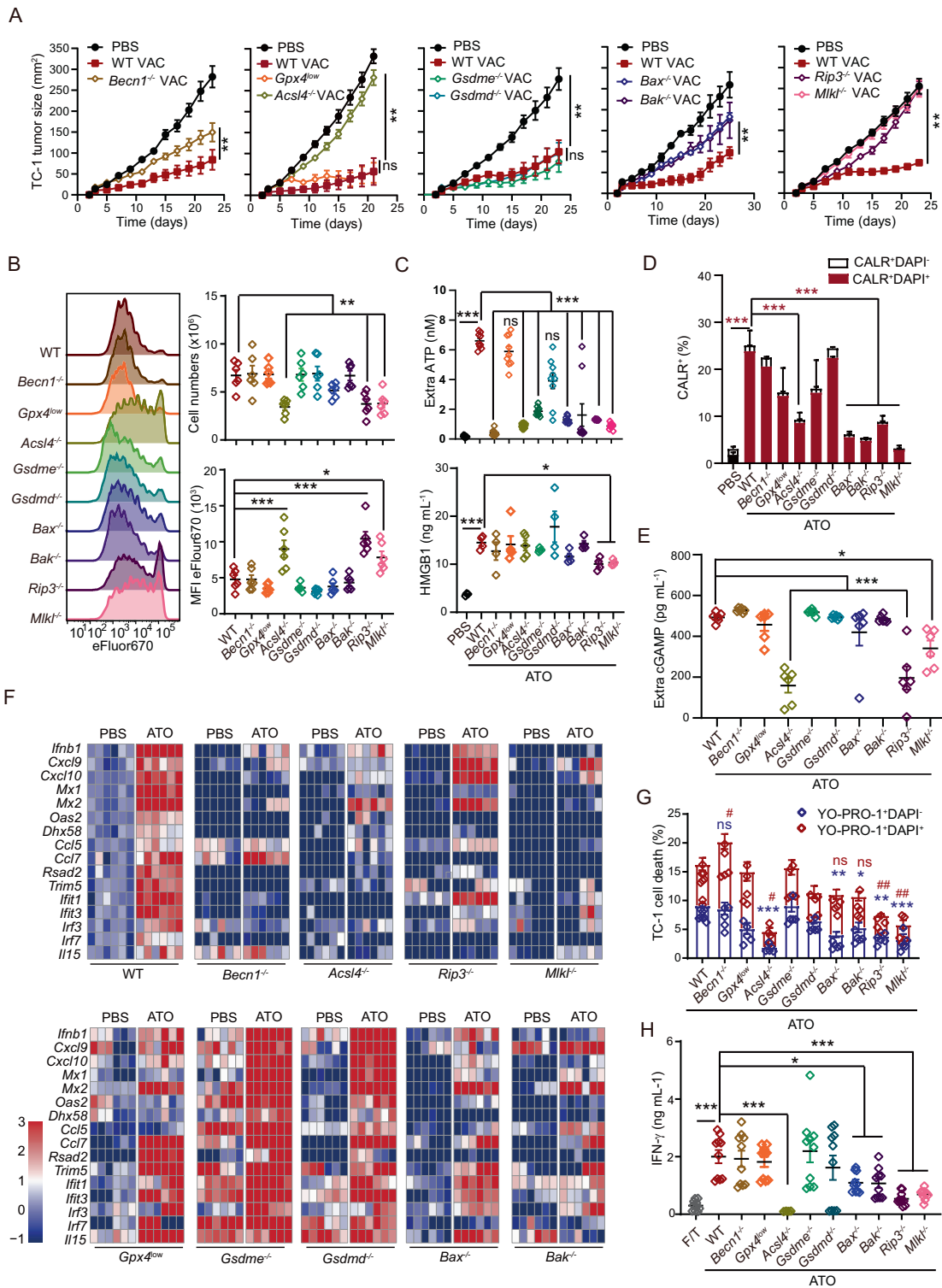


Fig. 5 The contributions of different cell death executors to ATO-induced ICD and the benefits of prophylactic vaccines. **A** WT or KO TC-1 cells (*Becn1*^{-/-}, *Gpx4*^{low}, *Acs14*^{-/-}, *Gsdme*^{-/-}, *Gsdmd*^{-/-}, *Gsdme*^{-/-}, *Bax*^{-/-}, *Bak*^{-/-}, *Rip3*^{-/-} and *Mlkl*^{-/-}) were treated with ATO (25 μM, 16 h) and utilized as prophylactic vaccines in naïve mice. Tumor growth was monitored for each individual mouse after tumor rechallenge with WT TC-1 cells (n = 5–7). **B** ATO-preconditioned WT or KO TC-1 cells were injected s.c. into the footpad to stimulate adoptively transferred OT-1 cells. Representative histograms illustrate the proliferation of eFluor670-labeled OT-1 cells in vivo. Statistical analyses of the OT-1 cell number in the draining lymph nodes and associated MFI are shown (n = 6). **C–F** The ATO-induced generation and release of a series of ICD factors, such as ATP, HMGB1 (**C**, n = 4–9), CALR exposure (**D**, n = 3), cGAMP release (**E**, n = 6), and the expression of ISGs (**F**, n = 6), were compared between WT and KO TC-1 cells. **G** The ATO-induced disruption of membrane integrity was compared between WT and KO TC-1 cells, as determined by YO-PRO-1/DAPI dual staining (n = 6). **H** In vitro tumor antigen presentation assays were performed with ATO-treated WT or KO TC-1 cells, which were cocultured with BMDCs and OT-1 cells for 3 days (n = 9). Data are shown as the mean ± SEM. # p < 0.05, ** or ## p < 0.01, *** p < 0.001; ns not significant

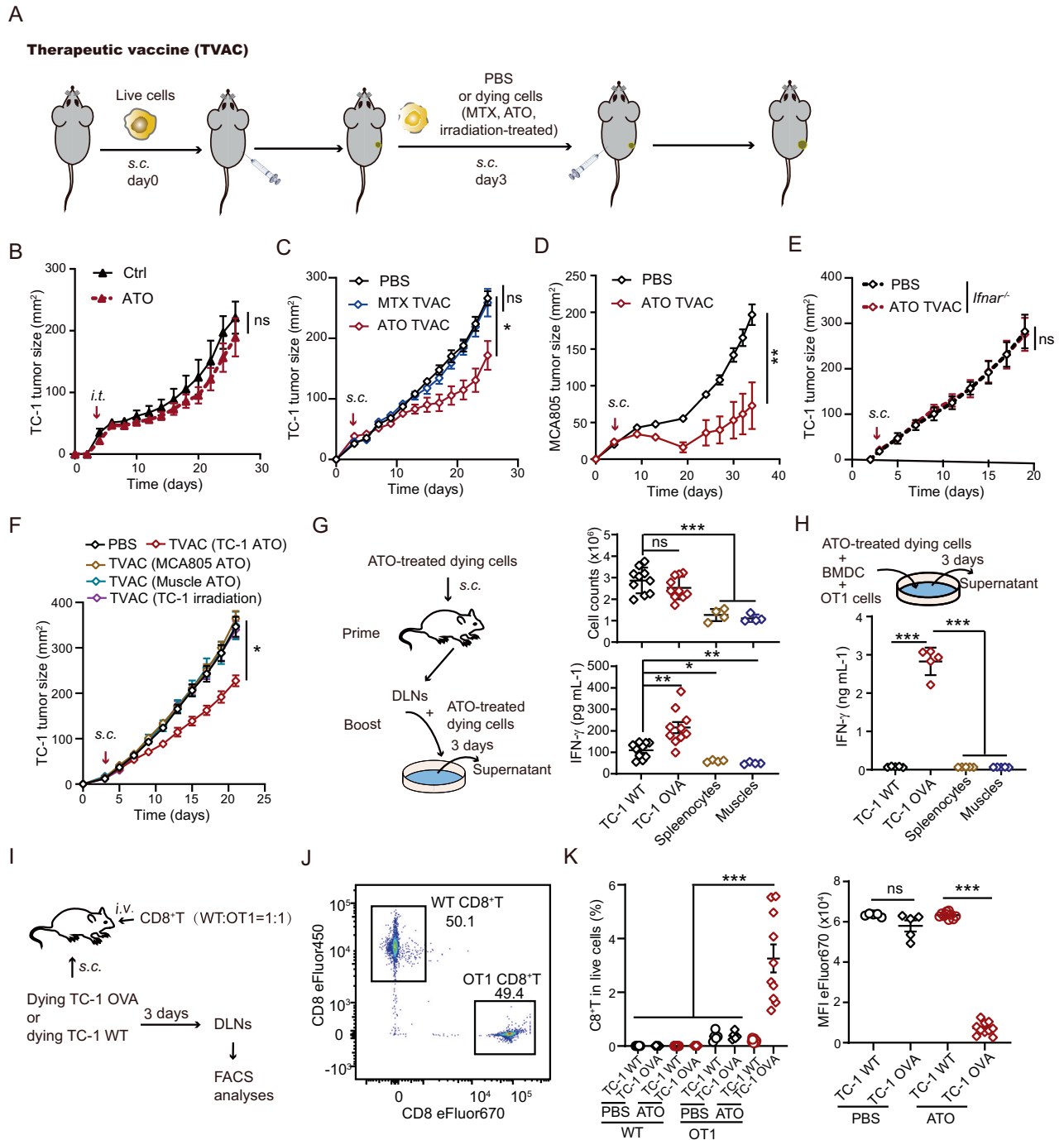


Fig. 6 ATO-based whole-cell vaccines exert therapeutic effects and elicit antitumor immunity. **A** Schematic diagram showing the therapeutic tumor vaccine regimen. **B** Tumor growth was monitored in TC-1 cell-bearing mice after intratumoral injection of either ATO or PBS control ($n = 4-5$). Different doses of ATO were tested, and a data summary is included in Fig. S6. **C, D** The efficacy of MTX- or ATO-based whole-cell vaccines against TC-1 (**C**) or MCA805 (**D**) tumors ($n = 5-6$) was compared in immunocompetent WT mice. **E** The efficacy of an ATO-based therapeutic vaccine (TVAC) against TC-1 tumors was tested in *Ifnar^{-/-}* mice ($n = 8$). **F** The therapeutic benefits of different TVACs (ATO-treated TC-1 cells, MCA805 cells or muscle cells, or X-ray-irradiated TC-1 cells) against existing TC-1 tumors were compared. **G** Schematic diagram showing the prime-boost regimen (left panel). The total cell number in the draining lymph nodes and tumor antigen-stimulated IFN- γ production were quantified ($n = 4-10$). **H** Schematic diagram showing the in vitro antigen presentation regimen (upper panel). Different types of ATO-treated dying cells were cocultured with BMDCs and OT-1 cells. IFN- γ secretion by the cell mixture was measured by ELISA 3 days later (lower panel, $n = 5$). **I-K** Schematic diagram showing the in vivo T-cell competition assay (**I**). WT and OT-1 CD8⁺ T cells were prestained with eFluor450 and eFluor670, respectively. The cells were adoptively transferred into WT recipient mice at a 1:1 ratio, as validated by flow cytometry (**J**). Three days after subcutaneous injection of PBS- or ATO-treated tumor cells (TC-1 WT or TC-1 OVA) into these mice, the frequency of infused OT-1 CD8⁺ T cells in the draining lymph nodes and their proliferation were analyzed by flow cytometry (**K**, $n = 10$). All data are shown as the mean \pm SEM. * $p < 0.05$, ** $p < 0.01$, *** $p < 0.001$; ns not significant

activities against TC-1 tumors in vivo (Fig. 6F, S6I). In an ex vivo antigen presentation assay with BMDCs, ATO-treated TC-1 OVA cells potentially elicited IFN- γ secretion by OT-1 cells. However, ATO-treated TC-1 WT cells (lacking the antigen OVA) or nonmalignant cells (splenocytes and muscle cells) failed to reproduce this phenomenon (Fig. 6G, H). In a T-cell competition assay, CD8⁺ T cells were purified from the spleen of WT or OT-1 mice, labeled with a fluorescent dye (eFlour450 or eFlour670), mixed at a 1:1 ratio, and adoptively transferred into WT recipient mice (Fig. 6I, J). These mice also received subcutaneous injection of ATO-treated dying tumor cells (TC-1 WT or TC-1 OVA). Three days later, the frequency of OT-1 cells and their proliferation in the draining lymph nodes were significantly higher than those of transferred WT CD8⁺ T cells (Fig. 6K, S6J). Therefore, the antitumor immunity elicited by an ATO-based whole-cell vaccine is antigen specific and not broad spectrum.

Consistent with the prophylactic vaccine setting, key executors of ferroptosis and necroptosis were also indispensable for the tumor growth-inhibitory effect of ATO-based therapeutic vaccines (Fig. 7A, S7A). By analyzing the frequencies of tumor-infiltrating immune cells with flow cytometry (Fig. S7B, C), we found that the therapeutic failure of *Rip3*^{-/-}, *Mkl1*^{-/-}, and *Acs14*^{-/-} whole-cell vaccines correlated with significantly reduced levels of CD3⁺ T cells, CD4⁺ helper T cells, CD8⁺ cytotoxic T cells, natural killer (NK) cells, macrophages, and DCs in the TME (Fig. 7B, C). Moreover, the expression of an early activation marker (CD69) and effector cytokines (IFN- γ and TNF- α) by tumor-infiltrating CD8⁺ and CD4⁺ T cells was much lower in the *Rip3*^{-/-}, *Mkl1*^{-/-}, and *Acs14*^{-/-} groups than in the WT group (Fig. 7D, E). Importantly, the therapeutic efficacy of the ATO-based *Rip3*^{-/-} whole-cell vaccine was rescued by coadministration of ICD factor analogs, including the apyrase inhibitor ARL67156, the TLR4 agonist MPLAs, and the STING agonist 2'3'-cGAMP (abbreviated as AMC) (Fig. 7F, S7D). The immunosuppressive TME is a major obstacle to boosting vaccine-elicited antitumor immunity. Therefore, we tried to combine this therapeutic vaccine approach with immune checkpoint inhibitors. Indeed, anti-PD-1 and an ATO-based vaccine showed a strong synergistic effect in blocking tumor progression (Fig. 7G, S7E). This therapeutic advantage over monotherapy (either anti-PD-1 or vaccine alone) could be linked to the enormously increased secretion of IFN- γ by tumor-infiltrating T cells (Fig. 7H). We are in the process of combining this ATO-based vaccine regimen with other antineoplastic strategies, with the aim of expanding the therapeutic opportunities for cancer patients.

DISCUSSION

Accumulating evidence suggests that certain chemotherapeutic drugs, local irradiation, and oncolytic viruses can trigger ICD and act as 'in situ vaccines' to stimulate tumor immunosurveillance [12, 13, 42, 43]. Prompted by these encouraging discoveries, we screened for strong ICD inducers and identified ATO as a top candidate. Although ATO (alone or combined with ATRA) has revolutionarily made APL curable, its therapeutic benefits in solid tumors are quite limited. Moreover, ATO often causes severe side effects, making it intolerable in cancer patients. Hence, we tested the possibility of dissociating the beneficial ICD-inducing property of ATO from its undesirable cytotoxicity to healthy tissues. In our study, ATO preconditioning ex vivo not only killed tumor cells but also largely increased their antigenicity and adjuvanticity. Once inoculated as vaccines in mice, these dying tumor cells exhibited both prophylactic and therapeutic activities and significantly reduced tumor outgrowth (Figs. 2B, C, 6C, D). We did not observe any signs of overt inflammation or symptoms of autoimmunity.

A research focus in the therapeutic cancer vaccine field is the identification of highly immunogenic and specific tumor antigens and their dominant epitopes [9]. One of the pioneering studies showed that tumor vaccines designed to target up to 20 predicted

personal neoantigens led to durable antitumor responses in melanoma patients [44, 45], proving the feasibility and safety of targeting mutated proteins and neoantigen epitopes rather than weakly immunogenic nonmutated tumor-associated antigens [46]. Our work suggests that tumor cells undergoing ICD also display encouraging therapeutic potential, since they retain a complete repertoire of tumor antigens (and thus are naturally multivalent) and concomitantly generate multiple immunostimulatory ICD factors (with strong adjuvanticity). Indeed, the ATO-based whole-cell vaccine could switch immunologically 'cold' tumors to 'hot' tumors by improving the infiltration of T cells, NK cells, and DCs and promoting the secretion of IFN- γ and TNF- α by T cells (Fig. 7B–E). It could also enhance the proliferation of tumor antigen-specific T cells in the vaccine-draining lymph nodes (Fig. 1C). Consistently, depleting CD8⁺ T cells (rather than NK cells) or blocking type I or II IFN signaling abolished the tumor growth-inhibitory effects of this vaccine regimen (Figs. 2D–L, 6E).

To our surprise, ATO treatment simultaneously activated multiple pathways involved in the cellular stress response and death, as revealed by comprehensive kinetic analyses of key executors and biomarkers (Fig. 4D). The physiopathological and therapeutic implications of different cell death modalities, as well as their coordination and antagonism, are core issues in the field of cell death. In our study, *Rip3*- and *Mkl1*-dependent necroptosis and *Acs14*-dependent ferroptosis were required for the prophylactic and therapeutic efficacy of ATO-based whole-cell vaccines, while *Becn1*-dependent autophagy and *Bax*- and *Bak*-dependent apoptosis also contributed to vaccine-induced tumor restriction (Figs. 5A, 7A). This finding could be explained by the fact that the absence of necroptosis or ferroptosis executors generally abrogated the release of multiple ICD factors, presumably due to the reduced membrane permeabilization in *Acs14*^{-/-}, *Rip3*^{-/-}, and *Mkl1*^{-/-} tumor cells upon ATO treatment (Fig. 5G). Similar to previous reports, autophagy and apoptosis machineries were necessary for the release of ATP from dying tumor cells [29], whereas the accumulation of extracellular HMGB1 was mostly influenced by the necroptotic pathway [30]. We discovered that ferroptosis, apoptosis and necroptosis were requisites for the surface exposure of CALR, whereas the release of cGAMP preferentially relied on ferroptosis and necroptosis. In addition, the autophagic, apoptotic, necroptotic, and ferroptotic pathways were required for ATO-induced type I IFN responses (Fig. 5C–F).

Chemotherapeutic drugs and inflammatory stimuli were reported to augment ROS production and induce pyroptosis via CASP-mediated cleavage of gasdermins [47, 48]. Interestingly, cleaved GSDME can permeabilize the mitochondria, release cytochrome c, and promote CASP3 activation [49]. Thus, it may initiate a positive feedback loop that favors pyroptosis. Unexpectedly, ATO treatment led to a gradual loss of full-length GSDMD and GSDME, but their cytolytic N-terminal fragments were not detectable (Fig. 4D). Autophagy was reported to counteract pyroptosis via the p62-mediated degradation of GSDMD [50]. ATO treatment initiated autophagy as early as 2 h, long before apoptosis occurred (8 h) (Fig. 4D). Coincidentally, the degradation of GSDMD and GSDME took place between 2–8 h (Fig. 4D), implying that the autophagic–lysosomal system might participate in this process. Nevertheless, blocking the fusion of autophagosomes and lysosomes with bafilomycin A1 could not inhibit the degradation of these gasdermins. It seemed that neither the ubiquitin–proteasome system nor CASP proteases contributed to the loss of GSDMD and GSDME (Fig. S4C). Instead, the ROS-mediated oxidation degradation pathway appeared to be a crucial regulator of the half-life of gasdermins (Fig. 4D), although the underlying mechanisms remained elusive.

To improve the therapeutic benefits of this ATO-based whole-cell vaccine and rationalize its clinical applications, efforts need to be made in three areas: (1) overcome the intrinsic defects in the immunogenicity of autologous cancer cells by compensating for

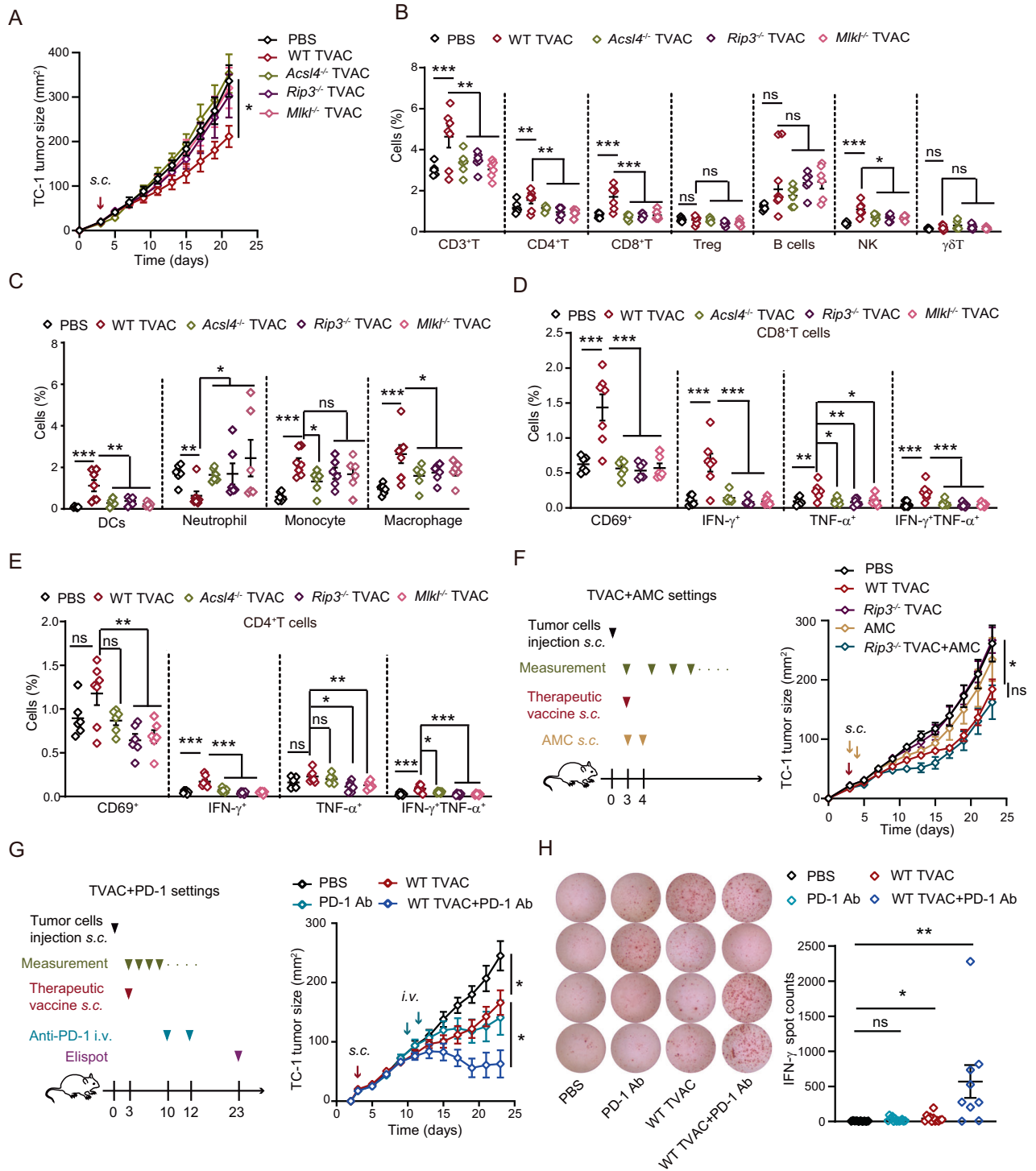


Fig. 7 ATO-based TVACs reshape the tumor immune microenvironment and combinatorial approaches for their optimization. **A** WT and KO cells (*Acs14*^{-/-}, *Rip3*^{-/-}, and *Mki1*^{-/-}) were used to generate ATO-based TVACs, and their efficacy was compared (*n* = 6–7). **B–E** Twelve days after injection of the indicated TVAC, the proportions of tumor-infiltrating immune cell subsets (**B, C**), the expression of CD69, and the production of cytokines (**D, E**) were analyzed by FACS (*n* = 6–7). **F** A mixture of ICD factor analogs (abbreviated as AMC) was combined with a *Rip3*^{-/-}-based TVAC (as shown by the scheme). The therapeutic outcome was compared with that of monotherapies or PBS control (as shown by the tumor growth curves in the right panel). **G, H** Mice bearing TC-1 tumors were treated with TVAC immunization and/or PD-1 blockade at the indicated time points. The tumor growth kinetics were recorded for each individual (**G**, *n* = 6–7). Intratumoral IFN-γ production was quantified by ELISpot assays and compared among mice that received anti-PD-1 monotherapy, TVAC monotherapy, or combination therapy. Typical images of ELISpot assays and statistical analyses are shown (**H**, *n* = 10–12). All data are shown as the mean ± SEM. **p* < 0.05, ***p* < 0.01, ****p* < 0.001; ns not significant

key cell death executors, ICD factor mimetics, or immunostimulatory cytokines; (2) expand the therapeutic window to middle- and late-stage cancers through treatment in combination with other immunotherapeutic approaches; and (3) establish a strict quality-control system to guarantee high immunogenicity and complete loss of oncogenic potential.

DATA AVAILABILITY

All requests for raw and analyzed data and materials will be promptly reviewed by the Institute of Systems Medicine, Chinese Academy of Medical Sciences, to verify whether the request is subject to any intellectual property or confidentiality obligations. Any data and materials that can be shared will be released via a material transfer agreement. All raw RNA-sequencing data can be found at the NCBI Sequence Read Archive (accession number: PRJNA818773).

REFERENCES

- Song M, Vogelstein B, Giovannucci EL, Willett WC, Tomasetti C. Cancer prevention: molecular and epidemiologic consensus. *Science*. 2018;361:1317–8. <https://doi.org/10.1126/science.aau3830>
- Finn OJ. The dawn of vaccines for cancer prevention. *Nat Rev Immunol*. 2018;18:183–94. <https://doi.org/10.1038/nri.2017.140>
- Garland SM, Kjaer SK, Munoz N, Block SL, Brown DR, DiNubile MJ, et al. Impact and effectiveness of the quadrivalent human papillomavirus vaccine: a systematic review of 10 years of real-world experience. *Clin Infect Dis*. 2016;63:519–27. <https://doi.org/10.1093/cid/ciw354>
- McMahon BJ, Bulkow LR, Singleton RJ, Williams J, Snowball M, Homan C, et al. Elimination of hepatocellular carcinoma and acute hepatitis B in children 25 years after a hepatitis B newborn and catch-up immunization program. *Hepatology*. 2011;54:801–7. <https://doi.org/10.1002/hep.24442>
- Sun X, Zeng L, Huang Y. Transcutaneous delivery of DNA/mRNA for cancer therapeutic vaccination. *J Gene Med*. 2019;21:e3089. <https://doi.org/10.1002/jgm.3089>
- Peng M, Mo Y, Wang Y, Wu P, Zhang Y, Xiong F, et al. Neoantigen vaccine: an emerging tumor immunotherapy. *Mol Cancer*. 2019;18:128. <https://doi.org/10.1186/s12943-019-1055-6>
- Jou J, Harrington KJ, Zocca MB, Ehrnrooth E, Cohen EEW. The changing landscape of therapeutic cancer vaccines—novel platforms and neoantigen identification. *Clin Cancer Res*. 2021;27:689–703. <https://doi.org/10.1158/1078-0432.CCR-20-0245>
- Cheever MA, Higano CS. PROVENGE (Sipuleucel-T) in prostate cancer: the first FDA-approved therapeutic cancer vaccine. *Clin Cancer Res*. 2011;17:3520–6. <https://doi.org/10.1158/1078-0432.CCR-10-3126>
- Saxena M, van der Burg SH, Melief CJM, Bhardwaj N. Therapeutic cancer vaccines. *Nat Rev Cancer*. 2021;21:360–78. <https://doi.org/10.1038/s41568-021-00346-0>
- van der Burg SH, Arens R, Ossendorp F, van Hall T, Melief CJ. Vaccines for established cancer: overcoming the challenges posed by immune evasion. *Nat Rev Cancer*. 2016;16:219–33. <https://doi.org/10.1038/nrc.2016.16>
- Zitvogel L, Apetoh L, Ghiringhelli F, Kroemer G. Immunological aspects of cancer chemotherapy. *Nat Rev Immunol*. 2008;8:59–73. <https://doi.org/10.1038/nri2216>
- Ma Y, Kepp O, Ghiringhelli F, Apetoh L, Aymeric L, Locher C, et al. Chemotherapy and radiotherapy: cryptic anticancer vaccines. *Semin Immunol*. 2010;22:113–24. <https://doi.org/10.1016/j.smim.2010.03.001>
- Ma Y, Pitt JM, Li Q, Yang H. The renaissance of anti-neoplastic immunity from tumor cell demise. *Immunol Rev*. 2017;280:194–206. <https://doi.org/10.1111/imr.12586>
- Casares N, Pequignot MO, Tesniere A, Ghiringhelli F, Roux S, Chaput N, et al. Caspase-dependent immunogenicity of doxorubicin-induced tumor cell death. *J Exp Med*. 2005;202:1691–701. <https://doi.org/10.1084/jem.20050915>
- Min L, Teixeira A, Sanchez-Paulete AR, Ochoa MC, Alvarez M, Otano I, et al. Cellular cytotoxicity is a form of immunogenic cell death. *J Immunother Cancer*. 2020;8. <https://doi.org/10.1136/jitc-2019-000325>
- Vacchelli E, Ma Y, Baracco EE, Sistigu A, Enot DP, Pietrocola F, et al. Chemotherapy-induced antitumor immunity requires formyl peptide receptor 1. *Science*. 2015;350:972–8. <https://doi.org/10.1126/science.aad0779>
- Chiang CL, Benencia F, Coukos G. Whole tumor antigen vaccines. *Semin Immunol*. 2010;22:132–43. <https://doi.org/10.1016/j.smim.2010.02.004>
- Chiang CL, Coukos G, Kandalaf LE. Whole tumor antigen vaccines: where are we? *Vaccines (Basel)*. 2015;3:344–72. <https://doi.org/10.3390/vaccines3020344>
- Galaine J, Turco C, Vauchy C, Royer B, Mercier-Letondal P, Queiroz L, et al. CD4 T cells target colorectal cancer antigens upregulated by oxaliplatin. *Int J Cancer*. 2019;145:3112–25. <https://doi.org/10.1002/ijc.32620>
- Lhuillier C, Rudqvist NP, Yamazaki T, Zhang T, Charpentier M, Galluzzi L, et al. Radiotherapy-exposed CD8+ and CD4+ neoantigens enhance tumor control. *J Clin Invest*. 2021;131. <https://doi.org/10.1172/JCI138740>
- Rehman H, Silk AW, Kane MP, Kaufman HL. Into the clinic: Talimogene laherparepvec (T-VEC), a first-in-class intratumoral oncolytic viral therapy. *J Immunother Cancer*. 2016;4:53. <https://doi.org/10.1186/s40425-016-0158-5>
- Sasso MS, Mitrousis N, Wang Y, Briquez PS, Hauert S, Ishihara J, et al. Lymphangiogenesis-inducing vaccines elicit potent and long-lasting T cell immunity against melanomas. *Sci Adv*. 2021;7. <https://doi.org/10.1126/sciadv.abe436>
- Larocca CA, LeBoeuf NR, Silk AW, Kaufman HL. An update on the role of talimogene laherparepvec (T-VEC) in the treatment of melanoma: best practices and future directions. *Am J Clin Dermatol*. 2020;21:821–32. <https://doi.org/10.1007/s40257-020-00554-8>
- Stojdl DF, Lichty B, Knowles S, Marius R, Atkins H, Sonenberg N, et al. Exploiting tumor-specific defects in the interferon pathway with a previously unknown oncolytic virus. *Nat Med*. 2000;6:821–5. <https://doi.org/10.1038/77558>
- Laheru D, Lutz E, Burke J, Biedrzycki B, Solt S, Onners B, et al. Allogeneic granulocyte macrophage colony-stimulating factor-secreting tumor immunotherapy alone or in sequence with cyclophosphamide for metastatic pancreatic cancer: a pilot study of safety, feasibility, and immune activation. *Clin Cancer Res*. 2008;14:1455–63. <https://doi.org/10.1158/1078-0432.CCR-07-0371>
- Salgia R, Lynch T, Skarin A, Lucca J, Lynch C, Jung K, et al. Vaccination with irradiated autologous tumor cells engineered to secrete granulocyte-macrophage colony-stimulating factor augments antitumor immunity in some patients with metastatic non-small-cell lung carcinoma. *J Clin Oncol*. 2003;21:624–30. <https://doi.org/10.1200/JCO.2003.03.091>
- Chen Z, Chen SJ. Poisoning the Devil. *Cell*. 2017;168:556–60. <https://doi.org/10.1016/j.cell.2017.01.029>
- Lo-Coco F, Avvisati G, Vignetti M, Thiede C, Orlando SM, Iacobelli S, et al. Retinoic acid and arsenic trioxide for acute promyelocytic leukemia. *N Engl J Med*. 2013;369:111–21. <https://doi.org/10.1056/NEJMoa1300874>
- Michaud M, Martins I, Sukkurwala AQ, Adjemian S, Ma Y, Pellegatti P, et al. Autophagy-dependent anticancer immune responses induced by chemotherapeutic agents in mice. *Science*. 2011;334:1573–7. <https://doi.org/10.1126/science.1208347>
- Yang H, Ma Y, Chen G, Zhou H, Yamazaki T, Klein C, et al. Contribution of RIP3 and MLKL to immunogenic cell death signaling in cancer chemotherapy. *Oncotarget*. 2016;5:e1149673. <https://doi.org/10.1080/2162402X.2016.1149673>
- Wang Q, Wang Y, Ding J, Wang C, Zhou X, Gao W, et al. A bioorthogonal system reveals antitumor immune function of pyroptosis. *Nature*. 2020;579:421–6. <https://doi.org/10.1038/s41586-020-2079-1>
- Efimova I, Catanzaro E, Van der Meeren L, Turbanova VD, Hammad H, Mishchenko TA, et al. Vaccination with early ferroptotic cancer cells induces efficient antitumor immunity. *J Immunother Cancer*. 2020;8. <https://doi.org/10.1136/jitc-2020-001369>
- Liao P, Wang W, Wang W, Kryczek I, Li X, Bian Y, et al. CD8(+) T cells and fatty acids orchestrate tumor ferroptosis and immunity via ACSL4. *Cancer Cell*. 2022. <https://doi.org/10.1016/j.ccell.2022.02.003>
- Michaud M, Sukkurwala AQ, Di Sano F, Zitvogel L, Kepp O, Kroemer G. Synthetic induction of immunogenic cell death by genetic stimulation of endoplasmic reticulum stress. *Oncotarget*. 2014;3:e28276. <https://doi.org/10.4161/onc.128276>
- Aaes TL, Kaczmarek A, Delvaeye T, De Craene B, De Koker S, Heyndrickx L. Vaccination with necroptotic cancer cells induces efficient anti-tumor immunity. *Cell Rep*. 2016;15:274–87. <https://doi.org/10.1016/j.celrep.2016.03.037>
- Obeid M, Tesniere A, Ghiringhelli F, Fimia GM, Apetoh L, Perfettini JL. Calreticulin exposure dictates the immunogenicity of cancer cell death. *Nat Med*. 2007;13:54–61. <https://doi.org/10.1038/nm1523>
- Wang Y, Gao W, Shi X, Ding J, Liu W, He H, et al. Chemotherapy drugs induce pyroptosis through caspase-3 cleavage of a gasdermin. *Nature*. 2017;547:99–103. <https://doi.org/10.1038/nature22393>
- Sarhan J, Liu BC, Muendlein HI, Li P, Nilson R, Tang AY, et al. Caspase-8 induces cleavage of gasdermin D to elicit pyroptosis during *Yersinia* infection. *Proc Natl Acad Sci USA*. 2018;115:E10888–97. <https://doi.org/10.1073/pnas.1809548115>
- Stutz A, Horvath GL, Monks BG, Latz E. ASC speck formation as a readout for inflammasome activation. *Methods Mol Biol*. 2013;1040:91–101. https://doi.org/10.1007/978-1-62703-523-1_8
- Lin CC, Hsu C, Hsu CH, Hsu WL, Cheng AL, Yang CH. Arsenic trioxide in patients with hepatocellular carcinoma: a phase II trial. *Invest N. Drugs*. 2007;25:77–84. <https://doi.org/10.1007/s10637-006-9004-9>
- Owonikoko TK, Zhang G, Kim HS, Stinson RM, Bechara R, Zhang C, et al. Patient-derived xenografts faithfully replicated clinical outcome in a phase II co-clinical trial of arsenic trioxide in relapsed small cell lung cancer. *J Transl Med*. 2016;14:111. <https://doi.org/10.1186/s12967-016-0861-5>
- Workenhe ST, Mossman KL. Oncolytic virotherapy and immunogenic cancer cell death: sharpening the sword for improved cancer treatment strategies. *Mol Ther*. 2014;22:251–6. <https://doi.org/10.1038/mt.2013.220>
- Deng L, Liang H, Xu M, Yang X, Burnette B, Arina A, et al. STING-dependent cytosolic DNA sensing promotes radiation-induced Type I interferon-dependent antitumor immunity in immunogenic tumors. *Immunity*. 2014;41:843–52. <https://doi.org/10.1016/j.immuni.2014.10.019>

44. Ott PA, Hu Z, Keskin DB, Shukla SA, Sun J, Bozym DJ, et al. An immunogenic personal neoantigen vaccine for patients with melanoma. *Nature*. 2017;547:217–21. <https://doi.org/10.1038/nature22991>
45. Hu Z, Leet DE, Allesoe RL, Oliveira G, Li S, Luoma AM, et al. Personal neoantigen vaccines induce persistent memory T cell responses and epitope spreading in patients with melanoma. *Nat Med*. 2021;27:515–25. <https://doi.org/10.1038/s41591-020-01206-4>
46. Wagner S, Mullins CS, Linnebacher M. Colorectal cancer vaccines: Tumor-associated antigens vs neoantigens. *World J Gastroenterol*. 2018;24:5418–32. <https://doi.org/10.3748/wjg.v24.i48.5418>
47. Zhang Z, Zhang H, Li D, Zhou X, Qin Q, Zhang Q. Caspase-3-mediated GSDME induced Pyroptosis in breast cancer cells through the ROS/JNK signalling pathway. *J Cell Mol Med*. 2021;25:8159–68. <https://doi.org/10.1111/jcmm.16574>
48. Jin Y, Li H, Xie G, Chen S, Wu S, Fang X. Sevoflurane combined with ATP activates caspase-1 and triggers caspase-1-dependent pyroptosis in murine J774 macrophages. *Inflammation*. 2013;36:330–6. <https://doi.org/10.1007/s10753-012-9550-6>
49. Rogers C, Rogers C, Erkes DA, Nardone A, Aplin AE. Gasdermin pores permeabilize mitochondria to augment caspase-3 activation during apoptosis and inflammasome activation. *Nat Commun*. 2019;10:1689. <https://doi.org/10.1038/s41467-019-09397-2>
50. Liao Z, Li S, Liu R, Feng X, Shi Y, Wang K, et al. Autophagic degradation of Gasdermin D protects against nucleus pulposus cell pyroptosis and retards intervertebral disc degeneration in vivo. *Oxid Med Cell Longev*. 2021;2021:5584447. <https://doi.org/10.1155/2021/5584447>

AUTHOR CONTRIBUTIONS

Study conception and design: YM. Data collection: JC, YM, SZ, ZJ, XZ. Analysis and interpretation of results: JC, YM, PL, HY. Draft manuscript preparation: YM, JC. All authors reviewed the results and approved the final version of the manuscript.

FUNDING

YM is supported by the National Science and Technology Innovation 2030 Major Project of China (2022ZD0205700), Natural Science Foundation of China (NSFC, 81972701), CAMS Innovation Fund for Medical Sciences (CIFMS; 2021-I2M-1-074, 2022-I2M-2-004), National Special Support Program for High-level Talents, China Ministry of Science and Technology (National Key Research and Development Program, Grant 2017YFA0506200), and Innovative and Entrepreneurial Team Program (Jiangsu Province).

COMPETING INTERESTS

The authors declare no competing interests.

ADDITIONAL INFORMATION

Supplementary information The online version contains supplementary material available at <https://doi.org/10.1038/s41423-022-00956-0>.

Correspondence and requests for materials should be addressed to Yuting Ma.

Reprints and permission information is available at <http://www.nature.com/reprints>

Springer Nature or its licensor (e.g. a society or other partner) holds exclusive rights to this article under a publishing agreement with the author(s) or other rightsholder(s); author self-archiving of the accepted manuscript version of this article is solely governed by the terms of such publishing agreement and applicable law.